ACS APPLIED MATERIALS & INTERFACES

Research Article

www.acsami.org

Strong Microwave Absorption of Hydrogenated Wide Bandgap Semiconductor Nanoparticles

Ting Xia,[†] Yinghui Cao,[‡] Nathan A. Oyler,[†] James Murowchick,[§] Lei Liu,*[,‡] and Xiaobo Chen*[,†]

[†]Department of Chemistry, University of Missouri−Kansas City, Kansas City, Missouri 64110, United States

[‡]State Key Laboratory of Luminescence and Applications, Changchun Institute of Optics, Fine Mechanics and Physics, Chinese Academy of Sciences, Changchun 130033, People's Republic of China

[§]Department of Geosciences, University of Missouri−Kansas City, Kansas City, Missouri 64110, United States

Supporting Information

ABSTRACT: Electromagnetic interactions in the microelectronvolt (μeV) or microwave region have numerous important applications in both civil and military fields, such as electronic communications, signal protection, and antireflective coatings on airplanes against microwave detection. Traditionally, nonmagnetic wide-bandgap metal oxide semiconductors lack these μeV electronic transitions and applications. Here, we demonstrate that these metal oxides can be fabricated as good microwave absorbers using a 2D electron gas plasma resonance at the disorder/order interface generated by a hydrogenation process. Using ZnO and TiO_2 nanoparticles as examples, we show that large absorption with reflection loss values as large as −49.0 dB (99.99999%) is obtained in the microwave region. The frequency of absorption can be tuned with the particle size and hydrogenation condition. These results may pave the way for new applications for wide bandgap semiconductors, especially in the μeV regime.

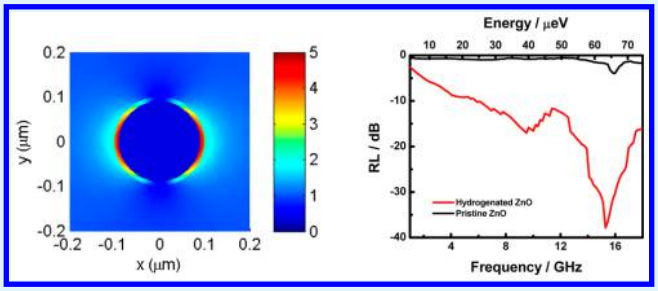

KEYWORDS: *electromagnetic absorption, wide bandgap, semiconductors, nanoparticles, 2D electron gas, plasmon*

INTRODUCTION

Microelectronvolt (μeV) electromagnetic radiation or microwaves play vital roles in our daily lives in providing for our community welfare and homeland security.[1−4] They are widely used in telecommunication, spacecraft communication, wireless communication, radar detection, and satellite navigation, among others.[1−4] Microwave coating materials with μeV absorption properties have been applied on electronics and devices to prevent signal leakage during communication and on aircraft to reduce radar detection in battlefields. Traditional coating materials include ferromagnetic nanoparticles[1,2] or conductive fillers in polymers.[3] Typical mechanisms for absorbing microwaves are electronic diffusive transport,[4] dipole rotations,[3,5] or ferromagnetic resonances.[1,2,6] Nonmagnetic wide-bandgap semiconductors are usually not good microwave absorbers. Blocked by the large energy bandgap in electron volts, their electronic transitions are not in tune with electromagnetic irradiation with energies much lower than their bandgaps. However, if fabricated into nanoscale heterostructures, their electronic states having quantized subband energy levels have been proven active in absorbing low-energy photons in the infrared,[7] or even terahertz regions.[8] Moreover, in response to electromagnetic radiation, low-energy plasma oscillations can be aroused from two-dimensional electron gas (2DEG) at the interfaces of semiconductor heterostructures as the terahertz detectors.[9,10] Unlike plasmons of bulk metals that show optical frequencies, plasmons in 2DEG of semiconductors behave differently: their frequency goes to zero as the wave vector goes zero and is tuned by the shape and dielectric properties of the semiconductors.[9,11] Therefore, in principle, 2DEG of semiconductors can also interact with even lower frequency electromagnetic waves, such as microwaves. In this study, we demonstrate that traditional wide-bandgap semiconductors can be fabricated with good microwave absorbing performance based on absorption by 2DEG plasmons at order/disorder's interfaces. As 2DEG plasmons have not been suggested for μeV microwave absorption, this work may lead to a new family of microwave absorbing materials.

RESULTS AND DISCUSSION

Theoretical Consideration. Historically, plasmons in 2DEG were first observed on the liquid helium surface,[12] in inversion layers of Si-SiO_2 structures,[11] and later on other semiconductor interfaces, such as AlGaAs\GaAs.[13] Due to the charge imbalance at interfaces between semiconductors, the bending of electronic bands may indeed form the quantum well structures, with typical widths on the order of 10 nm,[13] that

Received: February 19, 2015
Accepted: April 27, 2015
Published: April 27, 2015

© 2015 American Chemical Society

DOI: 10.1021/acsami.5b01598
ACS Appl. Mater. Interfaces 2015, 7, 10407−10413

effectively trap conductive electrons, forming a so-called 2DEG there. Usually, the heterostructures for producing such 2DEG are composed of two different semiconductors with alien dopants for energy offset of electronic bands and imbalanced charges. Recently, it was shown the heterostructure interfaces of semiconductors can be produced by hydrogenation-induced surface disorder.[14−17] The concept of hydrogenating nano-semiconductors with structural-disordered shells (i.e., "disorder-engineering"), was proposed for enhancing the photocatalytic activity of TiO_2 nanocrystals under solar radiation.[14,15] Because a band offset as large as 2.18 eV has been observed between the disordered surface and the crystalline core of TiO_2 nanocrystals,[14] 2DEG will naturally exist at their order/disorder interfaces, which in this case produces a spherical 2DEG. Unlike conventionally making 2DEG with semiconductor processing techniques, producing 2DEG with "disorder-engineering" here suggests a new way to chemically produce 2DEG electronics or plasmonics. Using TiO_2 and ZnO nanocrystals as examples, we show wide-bandgap semiconductors can be disorder-engineered into highly efficient microwave absorbers with 2DEG plasmons.

We have proposed a collective movement of interfacial dipole (CMID) mechanism with the core/shell TiO_2 nanoparticles in our previous study.[5] Here, the mechanism is further expanded to include the 2DEG-plasmon enhanced microwave absorption. It is well-known that the plasma frequency[18] of the free electron gas can be calculated by $\omega_p = (n_e e^2/\varepsilon_0 m^*)^{1/2}$, where n_e and m^* are the electron density and effective mass, respectively. For TiO_2 and ZnO, we set $m^* = 0.8m_e$ and $0.29m_e$ respectively,[19,20] and calculated their plasma frequency in bulk phase as shown in Figure 1A. As expected, Figure 1A demonstrates that if with an electron density of about 10^{13}/cm^3, the plasma frequency of both semiconductors falls in the microwave region. To examine the plasmon behavior of a spherical 2DEG, we employed a 2DEG shell model where the spherical semiconductor inclusions are ingrained into a pyroelectric matrix.[21] While a conductive sphere can support Mie plasmon modes, each of these modes splits into a doublet of spherelike and voidlike modes in a conductive shell.[22] Figure 1B,C presents the calculated electric-field distributions at the resonances of sphere-like and void-like modes for 2DEG constrained in spherical shell. Figure 1D presents the resonance plasmon frequency of sphere-like and void-like modes versus the ratio of inner and outer radii of the spherical shell, a_1/a_2. It is reasonable to approximate $a_1/a_2 = 0.9$ (the thickness of 2DEG is ∼10 nm and the radius of TiO_2 and ZnO is ∼100 nm); we then find the resonance plasmon frequency of 2DEG is about $0.1\omega_p$ and $0.4\omega_p$ for TiO_2 and ZnO nanocrystals, respectively. While ω_p scales monotonically on the electron density, in principle, the frequency of 2DEG plasmon in these disordered nanocrystals can be tuned to microwave region upon hydrogenation that donates electrons.

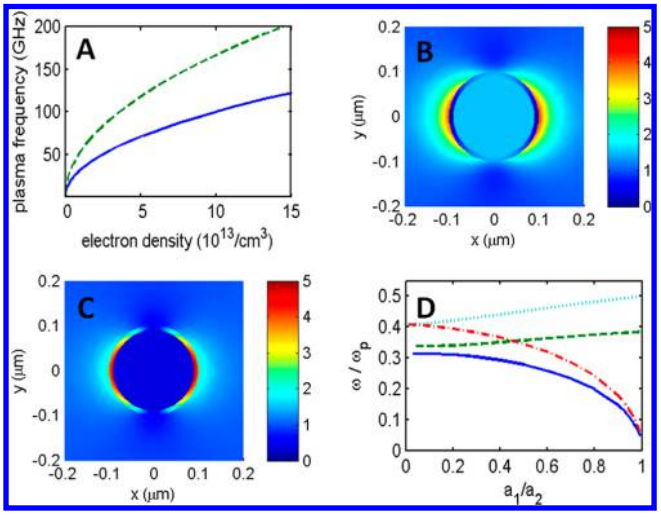

Figure 1. (A) Plasma frequency of the free electron gas in bulk TiO_2 (solid line) and ZnO (dashed line), respectively; Calculated electric-field distributions at the resonances of sphere-like (B) and void-like modes (C) for 2DEG constrained in spherical shell, with inner and outer radius of a_1 = 90 nm, a_2 = 100 nm; (D) The resonance frequency of sphere-like (solid line for TiO_2 and dashed line for ZnO) and void-like (dash-dotted line for TiO_2 and dotted line for ZnO) modes versus the ratio of inner and outer radius of the spherical shell, a_1/a_2.

Structural Properties. The 2DEG plasmon was experimentally produced on ZnO nanoparticles by heating under a high-pressure hydrogen atmosphere at high temperature. It directly induced a disordered lattice (Figure 2A) from the well-crystallized lattice in the pristine ZnO nanoparticle (Figure 2B), as seen in those high-resolution transmission electron microscopy (HRTEM) images. The hydrogenated nanoparticle did not reveal clear lattice fringes, while the pristine nanoparticle showed well-resolved lattice fringes and single crystalline nature. In contrast, heating pristine nanoparticles in air without hydrogen caused high crystallinity (Figure S1A, SI). In addition to the amorphization, particle growth to 150 nm (Figure 2C) was observed after hydrogenation from the small size of 15 nm of the pristine nanoparticles (Figure 2D), based on the low-resolution transmission electron microscopy (TEM) images. This growth was mainly due to the heating effect which was also observed on pristine ZnO nanoparticles heated in air (Figure S1B, SI).

The disordered lattice was confirmed with the weakened lattice vibrational features at around 115 and 459 cm^{-1} and increased defect-like luminescent background in their Raman spectrum (Figure 2E), in comparison to the strong peaks of pristine ZnO nanoparticles at around 115, 228, 350, 459, 697, 969, 1136, and 1479 cm^{-1}, attributed to the E_2^{low}, 2TA (A_1) ($2E_2^{low}$), A_1 (E_2, E_1), E_2^{high}, A_1 (2TO), A_1 (TO + LO), A_1(LO) and $2E_1$(LO) vibrational modes.[23] X-ray diffraction (XRD) examination revealed both nanoparticles had similar strong diffraction peaks (Figure 2F). The average crystalline grain size calculated using the Scherrer equation[14,24] showed 18.8 and 14.3 nm for hydrogenated and pristine ZnO nanoparticles, respectively. Heating pristine ZnO nanoparticles in air under the same condition gave a crystalline size of 19.1 nm (Figure S2, SI). Apparently, heating was responsible for such growth of crystalline grains as well. As the size of the nanoparticles was much larger than the crystalline grains after heating, aggregation apparently occurred during the heating. Because Raman is more surface sensitive than XRD, the aforementioned results suggested that the hydrogenated ZnO nanoparticles likely had a crystalline/amorphous core/shell structure, consistent with our previous findings in hydrogenated black TiO_2 nanoparticles.[14,16]

Dielectric Properties. The microwave absorption of hydrogenated ZnO nanoparticles was studied by examining their complex permittivity and permeability in the frequency range of 1−18 GHz. The real part ε' and μ' are related to the stored electrical and magnetic energy within the medium; the

DOI: 10.1021/acsami.5b01598
ACS Appl. Mater. Interfaces 2015, 7, 10407−10413

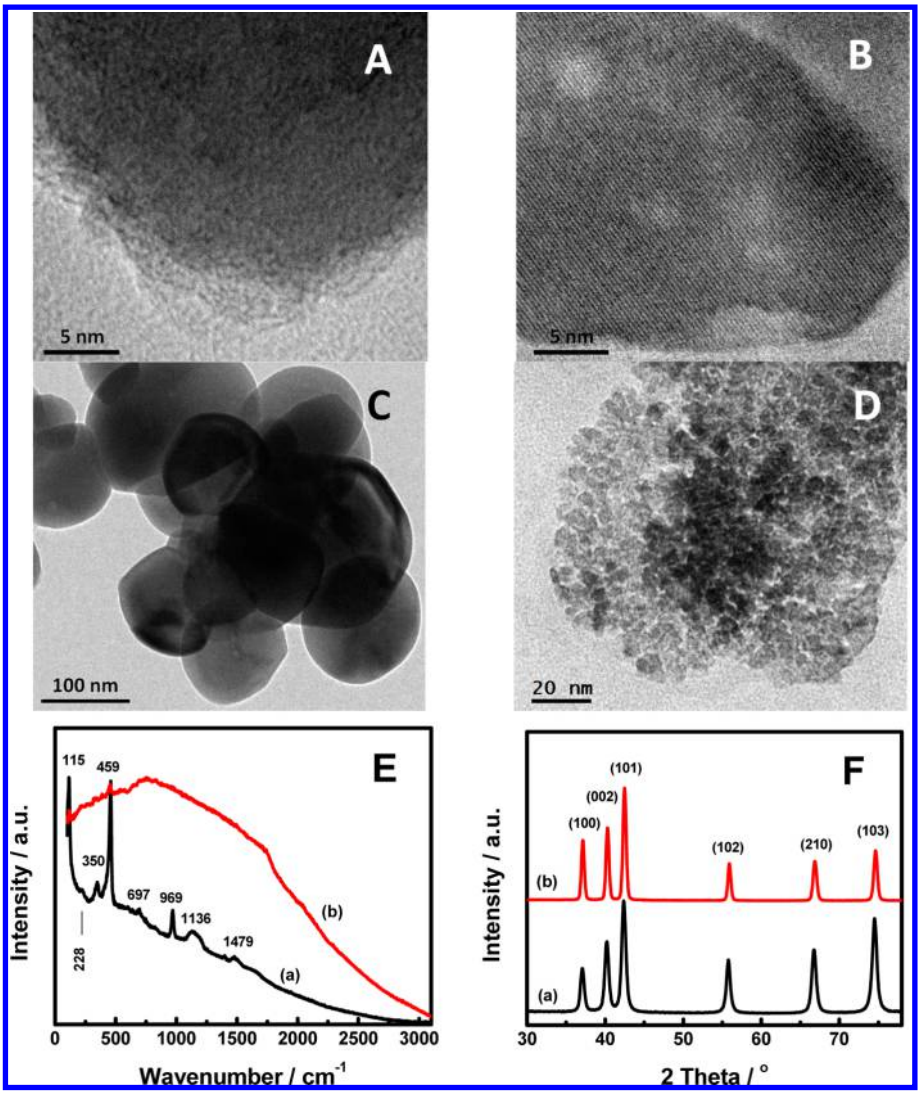

Figure 2. HRTEM images of (A) hydrogenated and (B) pristine ZnO nanoparticles, TEM images of (C) hydrogenated and (D) pristine ZnO nanoparticles, (E) Raman spectra and (F) XRD patterns of (a) pristine and (b) hydrogenated ZnO nanoparticles.

imaginary part ε'' and μ'' are related to the dissipation (or loss) of electrical and magnetic energy; their ratios and the dielectric and magnetic dissipation factors, $tg\delta_\varepsilon = \varepsilon''/\varepsilon'$ and $tg\delta_\mu = \mu''/\mu'$, provide a measure of how much power is lost in a material versus how much is stored.[25−28]

Much higher ε' and ε'' values were achieved after hydrogenation disorder perturbation (Figure 3A). This was consistent with the proposed 2DEG in the theoretical section that large changes of dielectric constants were expected at the interfaces of the crystalline/amorphous core/shell structure of hydrogenated ZnO nanoparticles. The average ε' was around 13.0 (decreasing gradually from 15.4 at 1.0 GHz to 10.4 at 18.0 GHz), compared to 3.1 of the pristine ZnO nanoparticles/epoxy composites. A 21.5-fold increase was obtained after taking out the contribution of the epoxy (2.5 at X-band frequency[28]). The average ε'' value of hydrogenated ZnO nanoparticles/epoxy composites increased to 3.5 (gradually from 2.8 at 1.0 GHz to 4.4 at 18.0 GHz), from 0.03−0.1 (except 0.4 near 1 and 16 GHz) of the ZnO nanoparticles/epoxy composites (Figure 3B). A 44-fold increase was obtained after taking out the contribution of the epoxy (0−0.02 at X-band frequency[28]). These results suggested that the hydrogenated disorder perturbation caused large increases in both storing and dissipating the electrical energy of the μeV electromagnetic field. Meanwhile, only small changes were observed on μ' and μ'' upon hydrogenation. The μ' increased slowly from 0.92 at 1.0 GHz to 1.01 at 6.0 Hz and then decreased to 0.92 at 18.0 GHz, compared to the slight increase from 0.95 at 1.0 GHz to 1.02 at 18.0 GHz of pristine ZnO nanoparticles (Figure 3C). The μ'' values for both samples decreased as the frequency increased from about 0.45−0.50 at 1.0 GHz to 0.10 at 18.0 GHz (Figure 3D).

While disorder-hydrogenation mainly affected the permittivity rather than the permeability, the measurements of dissipation factors confirmed its dominant role in enhancing the dielectric performance of ZnO nanoparticles. The average $tg\delta_\varepsilon$ value was around 0.31 (0.11 at 1.0 GHz to 0.43 at 18.0 GHz), 10 times of that (0.03) of the pristine ZnO nanoparticles (Figure 3E). The $tg\delta_\mu$ value decreased slowly from 0.55 at 1.0 GHz to 0.10 at 18.0 GHz, slightly lower in the frequency region of 4.7−16.0 GHz but higher in other regions than that of pristine ZnO nanoparticles (Figure 3F). In contrast, heating ZnO nanoparticles in air did not bring large changes in the

DOI: 10.1021/acsami.5b01598
ACS Appl. Mater. Interfaces 2015, 7, 10407−10413

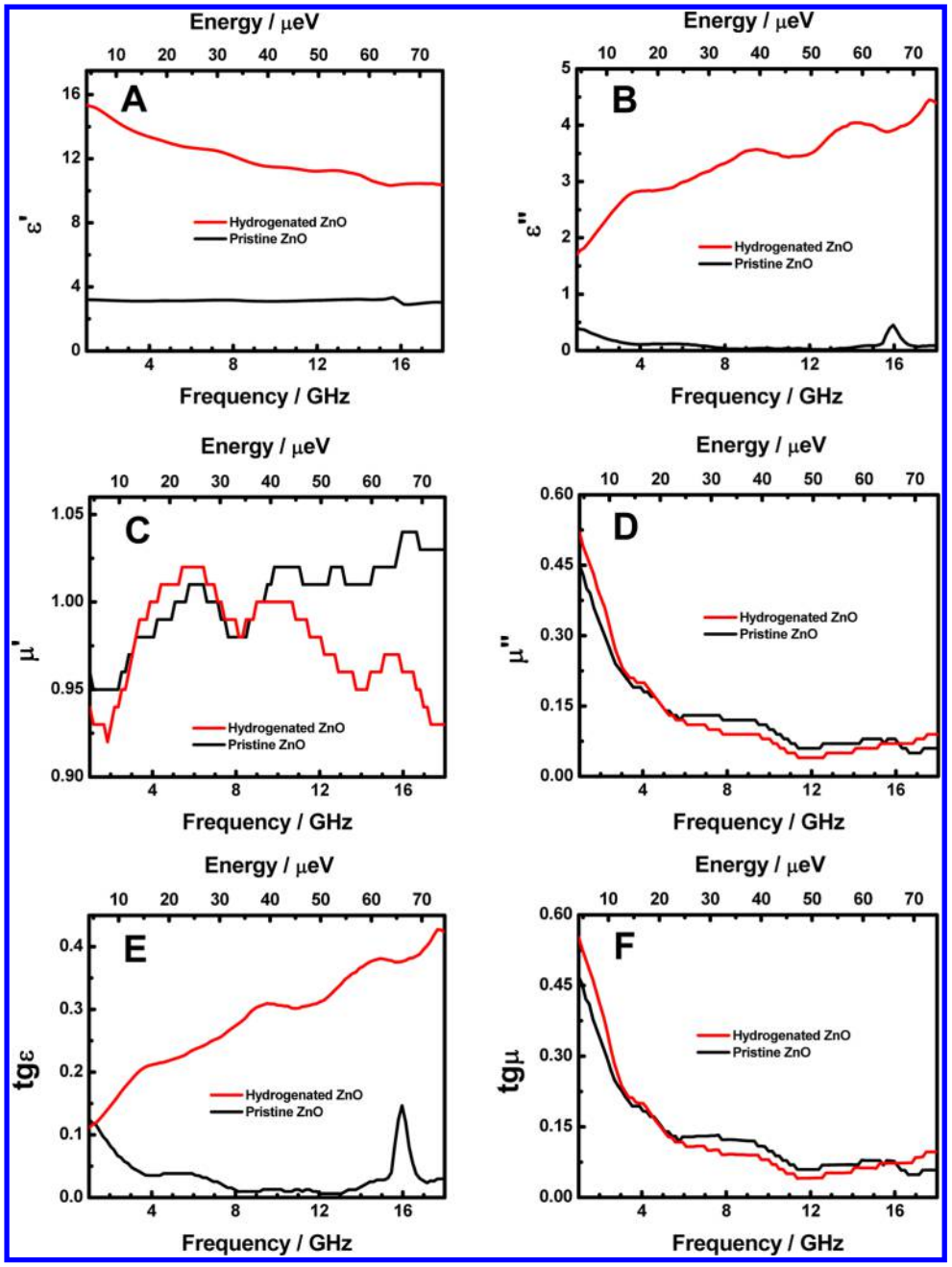

Figure 3. (A) Real part (ε') and (B) imaginary part (ε'') of the complex permittivity, (C) real part (μ') and (D) imaginary part (μ'') of the complex permeability, and (E) electrical (tgδ_ε) and (F) magnetic (tgδ_μ) dissipation factors in the microwave/μeV region of pristine and hydrogenated ZnO nanoparticles.

complex permittivity, permeability or the efficiency values across the same microwave frequency region (Figure S3, SI).

Microwave Absorption Performance. The electromagnetic reflection loss (RL) curves were calculated according to the following equations:[29]

$$Z_{in} = Z_0(\mu_r\varepsilon_r)^{1/2} \tanh\left[j(2\pi fd/c)(\mu_r\varepsilon_r)^{1/2}\right] \quad (1)$$

$$\mathrm{RL\ (dB)} = 20\log|(Z_{in} - Z_0)/(Z_{in} + Z_0)| \quad (2)$$

$$\mathrm{RL\ (dB)} = 10\log_{10}(P_i/P_r) \quad (3)$$

where f is the frequency of the electromagnetic wave, d is the thickness of the absorber, c is the velocity of light, Z_0 tis he impedance of free space, Z_{in} is the input impedance of the absorber, RL (dB) is the reflection loss, P_i is the incident power, and P_r is the reflected power. A material with a RL value of less than −30 is regarded as an excellent absorber, as this corresponds to 99.999% reflection loss or absorption. Ultimately, an ideal absorber would absorb 100% of the irradiation. Hydrogenated ZnO nanoparticles (with a thickness of 3.0 mm) showed very negative RL (dB) values in the range of 1.0−18.0 GHz with a valley value of −37.8 at around 15.3 GHz (Figure 4A), compared to a RL (dB) value of −0.5 (with a peak −4.0) at around 15.9 GHz of pristine ZnO nanoparticles. A RL (dB) value of −37.8 suggested a 99.9999% absorption, and a −4.0 responded to a 60% absorption. As expected, hydrogenated disorder largely improved the μeV absorption of ZnO nanoparticles. On the other hand, heating ZnO

DOI: 10.1021/acsami.5b01598
ACS Appl. Mater. Interfaces 2015, 7, 10407−10413

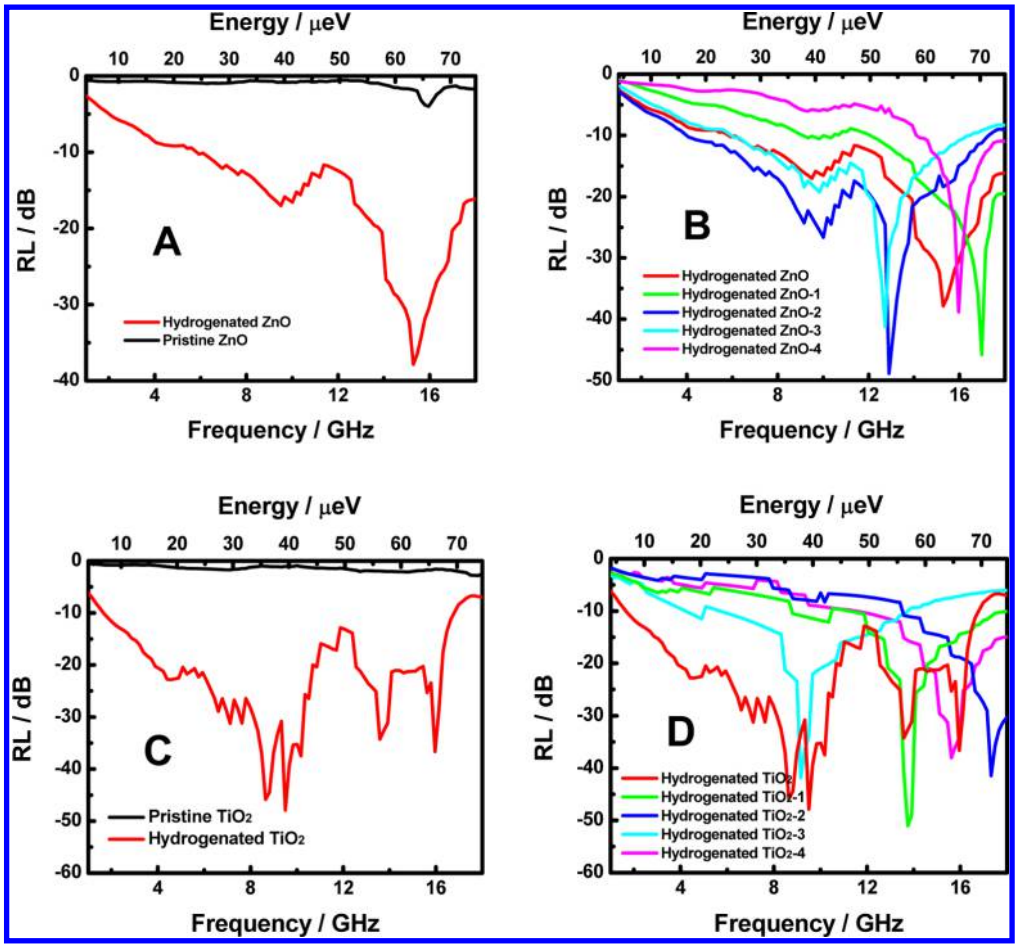

Figure 4. Reflection loss (RL) in the microwave/μeV region of pristine and hydrogenated (A) ZnO and (C) TiO_2 nanoparticles, hydrogenated (B) ZnO and (D) TiO_2 nanoparticles obtained under various hydrogenation conditions.

nanoparticles in air barely increased the absorption (Figure S4, SI).

To test the flexibility of this method, we fabricated a series of hydrogenated ZnO nanoparticles under different hydrogenation conditions and sizes. All hydrogenated ZnO nanoparticles displayed RL peak values more negative than −30 (Figure 4B), that is, they had excellent microwave absorbing performance. Upon size and hydrogenation variation, the frequency regions of the RL peaks of the hydrogenated ZnO nanoparticles can be tuned from 12.7 to 17.0 GHz, and the RL (dB) peak values can be tuned from −38.0 to −49.0. All the hydrogenated ZnO nanoparticles achieved 99.9999% reflection loss at particular frequencies in the microwave range. We further examined the same concept on TiO_2 nanoparticles. Similar enhancement in absorption has also been achieved in the microwave region for a series of hydrogenated TiO_2 nanoparticles (Figure 4C,D). The changes of frequency of microwave absorption of hydrogenated ZnO and TiO_2 nanoparticles prepared under various conditions demonstrate that the microwave absorption can be tuned with the particle size and hydrogenation condition. As these hydrogenated ZnO and TiO_2 nanoparticles were prepared by hydrogenation for various reaction times, their particle sizes changed correspondingly, resulting in variable structural properties, that is, the different parameters of the disordered/crystalline core/shell structures and, thus, different influences of the 2DEG on the dielectric constants and microwave absorption performance. In addition, based on previous studies,[3,27,28] the microwave absorption can be further tuned with the weight percentage of hydrogenated ZnO and TiO_2 nanoparticles within the paraffin wax.

Possibility of Other Mechanisms. Traditional mechanisms such as dipole rotation or ferromagnetic resonance do not seem to be valid here because neither permeability values nor dissipation factors of these nanoparticles show sensitive change after hydrogenation, and dipole rotation from polar groups did not induce good microwave absorption either. The lack of ferromagnetic resonance can be seen from the similar permeability values between the pristine and hydrogenated ZnO nanoparticles as shown in Figure 3. Fourier transform infrared measurements showed the disappearance of the OH vibrations after hydrogenation, compared to the obvious OH vibration centered at 3370 cm^{-1} (O−H stretching of strongly adsorbed H_2O[30,31] of pristine ZnO nanoparticles (Figure S5, SI). Instead, an increasing background absorption was observed with decreasing wavenumber, and the characteristic peaks at around 879, and 676 cm^{-1} of the Zn−O network became weak. These changes could be attributed to defects (e.g., oxygen vacancy or free electrons, hydrogen dopant) in the hydrogenated ZnO nanoparticles for increased charge concentration. Pristine ZnO nanoparticles had additional peaks from polar groups at around 1564 and 1430 cm^{-1} from C═O and C−O stretching, and peaks at 1338 and 1022 cm^{-1} separately label the C−O vibrations and the vibrations in the carboxylic ionic COO^- complex derived from the acetate precursor.[32] Although pristine ZnO nanoparticles had more polar groups, they display much poorer absorption in the microwave region.

DOI: 10.1021/acsami.5b01598
ACS Appl. Mater. Interfaces 2015, 7, 10407−10413

CONCLUSIONS

In summary, we have demonstrated that hydrogenated wide bandgap metal oxides (e.g., ZnO) can be fabricated with excellent microwave absorbing performance utilizing plasma resonance absorption at the disorder/order interface developed through a hydrogenation process. Large reflection loss or absorption (−49.0 dB RL, 99.99999% absorption) has been obtained in the microwave region. Moreover, the absorption frequency can be tuned with particle size and hydrogenation condition. These results may pave the way for new applications for wide-bandgap semiconductors, especially in the micro-electronvolt regime, for numerous civil and military applications.

METHODS

Calculation Details. According to Mie scattering theory,[22] the polarizability of 2DEG confined in a spherical shell can be taken as

$$\alpha = 4\pi a_2^3 \frac{(\varepsilon_2 - \varepsilon_m)(\varepsilon_1 + 2\varepsilon_2) + f(\varepsilon_1 - \varepsilon_2)(\varepsilon_m + 2\varepsilon_2)}{(\varepsilon_2 + 2\varepsilon_m)(\varepsilon_1 + 2\varepsilon_m) + f(2\varepsilon_2 - 2\varepsilon_m)(\varepsilon_1 - \varepsilon_2)}$$

where $f = (a_1/a_2)^3$; a_1 and a_2 are the inner and outer radius the spherical shell, respectively; and ε_1, ε_2, and ε_m are the permittivity in the core, the shell, and the surrounding medium, respectively. Here, according to the free electron model, the dielectric function of the free electron gas[18] can be written as $\varepsilon(\omega) = \varepsilon_\infty - \omega_p^2/(\omega^2 + i\gamma\omega)$, where γ is the collision frequency. The resonance condition of spherical 2DEG can be calculated by solving the equation:

$$(\varepsilon_2 + 2\varepsilon_m)(\varepsilon_1 + 2\varepsilon_m) + 2f(\varepsilon_2 - \varepsilon_m)(\varepsilon_1 - \varepsilon_2) = 0$$

where the permittivity of the shell ε_2 can be substituted as $\varepsilon_2 = \varepsilon_\infty - \omega_p^2/\omega^2$ in the case that γ is small. Here, $\varepsilon_1 = \varepsilon_\infty = 2.6$ is set for TiO_2, and $\varepsilon_1 = \varepsilon_\infty = 2.0$ for ZnO. We assume the surrounding medium is air, and thus, $\varepsilon_m = 1$.

Nanoparticle Synthesis. Pristine ZnO nanoparticles were prepared from a precursor solution consisting of sodium hydroxide, zinc acetate, ethanol, and water. The solution was stirred for 15 min, and the white precipitates were filtered, washed with deionized water, and dried to obtain ZnO nanoparticles. The TiO_2 nanoparticles were prepared following a previous method.[5] Hydrogenated and calcined nanoparticles were obtained by heating pristine nanoparticles under hydrogen and air atmospheres at 600 °C for 5 h. The pristine ZnO and TiO_2 nanoparticles were used as control groups to study the changes brought by the hydrogenation. Two series of hydrogenated ZnO and TiO_2 nanoparticles were prepared by heating ZnO and TiO_2 nanoparticles under hydrogen atmospheres for 1−4 h to demonstrate that the frequency of absorption can be tuned with the particle size and hydrogenation conditions. The samples were labeled as hydrogenated ZnO-1, -2, -3, -4 and hydrogenated TiO_2-1, -2, -3, -4, respectively.

Property Characterization. TEM was performed on an FEI Tecnai F200 transmission electron microscope. The electron accelerating voltage was at 200 kV. The Raman spectra were collected on an EZRaman-N benchtop Raman spectrometer with an excitation wavelength of 785 nm. XRD was performed using a Rigaku Miniflex XRD automated diffractometer using Cu Kα radiation and a Ni filter. The FTIR spectra were collected using a Thermo-Nicolet iS10 FT-IR spectrometer with an attenuated total reflectance (ATR) unit. ZnO nanoparticles were pressed onto the ZnSe crystal of the ATR unit, and the measurements were performed in air at room temperature.

The complex permittivity and permeability were measured using the waveguide technique at the frequency range of 1−18 GHz with a HP8722ES network analyzer.[5,28] The nanoparticles were dispersed in melted paraffin wax, and the mixture was cast into a ring mold with thickness of 2.0 mm, inner diameter of 3 mm, and outer diameter of 7 mm. The content of nanoparticles was 60 wt % in mass, and the testing was performed at room temperature. The microwave absorption performance curves were calculated with eqs 1 and 2 with the values of complex permittivity and permeability.

ASSOCIATED CONTENT

Supporting Information

The Supporting Information is available free of charge on the ACS Publications website at DOI: 10.1021/acsami.5b01598.

AUTHOR INFORMATION

Corresponding Authors

*E-mail: chenxiaobo@umkc.edu.
*E-mail: liulei@ciomp.ac.cn.

Author Contributions

T.X. and X.C. contributed to the synthesis of ZnO nanoparticles; Y.C. and L.L. performed the theoretical calculations; J.M. provided the XRD analysis; X.C. performed the other experiments and analysis; N.A.O. helped writing the manuscript; X.C. and L.L. wrote the paper with other authors' contribution.

Notes

The authors declare no competing financial interest.

ACKNOWLEDGMENTS

X.C. acknowledges the support of this research from the College of Arts and Sciences, University of Missouri−Kansas City (UMKC) and the University of Missouri Research Board. X.C. also thanks Mr. Yuan Ji and Professor Nicola Bowler at Iowa State University for discussion on microwave absorption measurements. L.L. acknowledges the support of the National Natural Science Foundation of China (No. 11174273).

REFERENCES

(1) Hewitt, W. H., Jr. Microwave Resonance Absorption in Ferromagnetic Semiconductors. *Phys. Rev.* **1948**, *73*, 1118.
(2) Qin, F.; Popov, V. V.; Peng, H.-X. Stress Tunable Microwave Absorption of Ferromagnetic Microwires for Sensing Applications. *J. Alloys Compd.* **2011**, *509*, 9508−9512.
(3) Qin, F.; Brosseau, C. A Review and Analysis of Microwave Absorption in Polymer Composites Filled with Carbonaceous Particles. *J. Appl. Phys.* **2012**, *111*, 061301/1−061301/24.
(4) Buniatyan, V. V.; Aroutiounian, V. M. Wide Gap Semiconductor Microwave Devices. *J. Phys. D: Appl. Phys.* **2007**, *40*, 6355−6385.
(5) Xia, T.; Zhang, C.; Oyler, N. A.; Chen, X. Hydrogenated TiO_2 Nanocrystals: A Novel Microwave Absorbing Material. *Adv. Mater.* **2013**, *25*, 6905−6910. Xia, T.; Zhang, C.; Oyler, N. A.; Chen, X. Enhancing Microwave Absorption of TiO_2 Nanocrystals via Hydrogenation. *J. Mater. Res.* **2014**, *29*, 2198−2210.
(6) Swarup, P.; Kumar, N. Microwave Faraday Rotation in Ferrite Powders. *Nature* **1964**, *204*, 947−948.
(7) Yao, Y.; Hoffman, A. J.; Gmachl, C. F. Mid-Infrared Quantum Cascade Lasers. *Nat. Photonics* **2012**, *6*, 432−439.
(8) Ferguson, B.; Zhang, X. C. Materials for Terahertz Science and Technology. *Nat. Mater.* **2002**, *1*, 26−33.
(9) Dyakonov, M.; Shur, M. Detection, Mixing, and Frequency Multiplication of Terahertz Radiation by Two-Dimensional Electronic Fluid. *IEEE Trans. Electron Devices* **1996**, *43*, 380−387.
(10) Sun, Y. F.; Sun, J. D.; Zhou, Y.; Tan, R. B.; Zeng, C. H.; Xue, W.; Qin, H.; Zhang, B. S.; Wu, D. M. Room Temperature GaN/AlGaN Self-Mixing Terahertz Detector Enhanced by Resonant Antennas. *Appl. Phys. Lett.* **2011**, *98*, 252103.
(11) Allen, S. J.; Tsui, D. C.; Logan, R. A. Observation of the Two-Dimensional Plasmon in Silicon Inversion Layers. *Phys. Rev. Lett.* **1977**, *38*, 980.

DOI: 10.1021/acsami.5b01598
ACS Appl. Mater. Interfaces 2015, 7, 10407−10413

(12) Grimes, C. C.; Adams, G. Observation of Two-Dimensional Plasmons and Electron-Ripplon Scattering in a Sheet of Electrons on Liquid Helium. *Phys. Rev. Lett.* **1976**, *36*, 145.
(13) Mannhart, J.; Blank, D. H. A.; Hwang, H. Y.; Millis, A. J.; Triscone, J. M. Two-Dimensional Electron Gases at Oxide Interfaces. *MRS Bull.* **2008**, *33*, 1027−1034.
(14) Chen, X.; Liu, L.; Yu, P. Y.; Mao, S. S. Increasing Solar Absorption for Photocatalysis with Black Hydrogenated Titanium Dioxide Nanocrystals. *Science* **2011**, *331*, 746−750.
(15) Liu, L.; Yu, P. Y.; Chen, X.; Mao, S. S.; Shen, D. Z. Hydrogenation and Disorder in Engineered Black TiO_2. *Phys. Rev. Lett.* **2013**, *111*, 065505/1−065505/5.
(16) Chen, X.; Liu, L.; Liu, Z.; Marcus, M. A.; Wang, W.-C.; Oyler, N. A.; Grass, M. E.; Mao, B.; Glans, P.-A.; Yu, P. Y.; Guo, J.; Mao, S. S. Properties of Disorder-Engineered Black Titanium Dioxide Nanoparticles through Hydrogenation. *Sci. Rep.* **2013**, *3*, 1510/1−1510/7.
(17) Liu, L.; Chen, X. Titanium Dioxide Nanomaterials: Self-Structural Modifications. *Chem. Rev.* **2014**, *114*, 9890−9918.
(18) Maier, S. A. *Plasmonics: Fundamentals and Applications*; Springer: New York, 2007.
(19) Baer, W. S. Faraday Rotation in ZnO − Determination of Electron Effective Mass. *Phys. Rev.* **1967**, *154*, 785−789.
(20) Enright, B.; Fitzmaurice, D. Spectroscopic Determination of Electron and Hole Effective Masses in a Nanocrystalline Semiconductor Film. *J. Phys. Chem.* **1996**, *100*, 1027−1035.
(21) Teperik, T. V.; García de Abajo, F. J.; Popov, V. V.; Shur, M. S. Strong Terahertz Absorption Bands in a Scaled Plasmonic Crystal. *Appl. Phys. Lett.* **2007**, *90*, 251910.
(22) Bohren, C.; Hufmann, D. *Absorption and Scattering of Light by Small Particles*; Wiley: New York, 1998.
(23) Harima, H. Raman Studies on Spintronics Materials Based on Wide Bandgap Semiconductors. *J. Phys. (Paris)* **2004**, *16*, S5653−S5660.
(24) Xia, T.; Chen, X. Revealing the Structural Properties of Hydrogenated Black TiO_2 Nanocrystals. *J. Mater. Chem. A* **2013**, *1*, 2983−2989.
(25) Petrov, V. M.; Gagulin, V. V. Microwave Absorbing Materials. *Inorg. Mater.* **2001**, *37*, 93−98.
(26) Micheli, D. *Radar Absorbing Materials and Microwave Shielding Structures Design*; Lambert Academic Publishing: Saarbrücken, Germany, 2012.
(27) Chen, Y. J.; Cao, M. S.; Wang, T. H.; Wan, Q. Microwave Absorption Properties of the ZnO Nanowire-Polyester Composites. *Appl. Phys. Lett.* **2004**, *84*, 3367−3369.
(28) Zhao, D. L.; Li, X.; Shen, Z. M. Microwave Absorbing Property and Complex Permittivity and Permeability of Epoxy Composites Containing Ni-Coated and Ag Filled Carbon Nanotubes. *Compos. Sci. Technol.* **2008**, *68*, 2902−2908.
(29) Matsumoto, M.; Miyata, Y. Thin Electromagnetic Wave Absorber for Quasi-Microwave Band Containing Aligned Thin Magnetic Metal Particles. *IEEE Trans. Magn.* **1997**, *33*, 4459−4464.
(30) Zou, J. A.; Gao, J. C.; Xie, F. Y. An Amorphous TiO_2 Sol Sensitized with H_2O_2 with the Enhancement of Photocatalytic Activity. *J. Alloys Compd.* **2010**, *497*, 420−427.
(31) Li, G. S.; Li, L. P.; Boerio-Goates, J.; Woodfield, B. F. High Purity Anatase TiO_2 Nanocrystals: Near Room-Temperature Synthesis, Grain Growth Kinetics, and Surface Hydration Chemistry. *J. Am. Chem. Soc.* **2005**, *127*, 8659−8666.
(32) Jakes, P.; Erdem, E. Finite Size Effects in ZnO Nanoparticles: An Electron Paramagnetic Resonance (EPR) Analysis. *Phys. Status Solidi* **2011**, *5*, 56−58.

DOI: 10.1021/acsami.5b01598
ACS Appl. Mater. Interfaces 2015, 7, 10407−10413